International Journal of Fracture 30 (1986) 237–259

Plastic near-tip fields for branched cracks

S. SURESH and C.F. SHIH

Division of Engineering, Brown University, Providence, RI 02912, USA

(Received 19 July 1985; in revised form 15 January 1986)

Abstract

A procedure is outlined whereby the plastic near-tip stress and deformation fields for branched cracks are determined under plane strain and small scale yielding conditions. This method utilizes the known elastic stress intensity factor solutions and the universal mixed-mode plastic near-tip fields to determine the stress and deformation conditions at the tip of a kinked or forked crack. The plastic near-tip fields are characterized by an amplitude and a mixity parameter. We examine the influence of crack tip plasticity and material strain hardening characteristics on the local stress and strain states. Possible beneficial effects of crack branching and crack tip plasticity on fracture toughness and crack growth resistance are discussed in the light of these results.

1. Introduction

It is now recognized that tensile cracks in engineering solids can deviate markedly from the nominal mode I crack plane due to a variety of mechanical, microstructural or environmental effects. Changes in crack path are generally induced by such factors as multiaxial far-field stresses, interaction of the crack tip with microstructural inhomogeneities, abrupt load excursions, or the embrittling effect of an aggressive environment. Several recent studies have examined the implications of crack branching to the fracture behavior of engineering materials [1–18]. The phenomena of crack kinking and forking can have a beneficial effect in the sense that they improve the fracture toughness as well as the resistance to crack growth. Figures 1a through 1e illustrate some examples of severely deflected crack profiles in ductile alloys during quasi-static fracture [14], constant amplitude fatigue fracture [15], variable amplitude fatigue fracture [16], environmentally-assisted (stress corrosion) fracture [17] and high temperature (creep) fracture [18], respectively.

Some of the beneficial effects of crack branching can be rationalized on the basis of elastic stress intensity factor solutions. A schematic of kinked and forked cracks is shown in Fig. 2. The nominal stress intensity factors K_I and K_{II} (based on the projected length c) and the crack tip stress intensity factors k_1 and k_2 are indicated in this figure. Numerous stress intensity factor solutions for kinked and forked cracks have been proposed [1–12] but there have been considerable disagreements (for a discussion, see [6,8]). In recent years consensus solutions appear to have been reached [5–9]. The stress intensity factors k_1 and k_2 for the kinked and forked cracks are smaller than the nominal stress intensity factors K_I and K_{II} (based on the projected length of the crack) and this suggests that beneficial effects can be expected. However there are cases where the measured improvement in the fracture toughness and crack growth resistance for cracks that kink and fork were very substantial; a closer examination of some of these cases revealed that the inferred plastic zone dimensions, though still small compared to the overall crack length, could be of the order of the size of the kink or fork (e.g. [14,15]).

It is a requirement of linear elastic fracture mechanics that the plastic zone be small compared to the relevant crack dimension. This condition implies that k_1 and k_2 are meaningful parameters for branched cracks only if the plastic zone is smaller than the

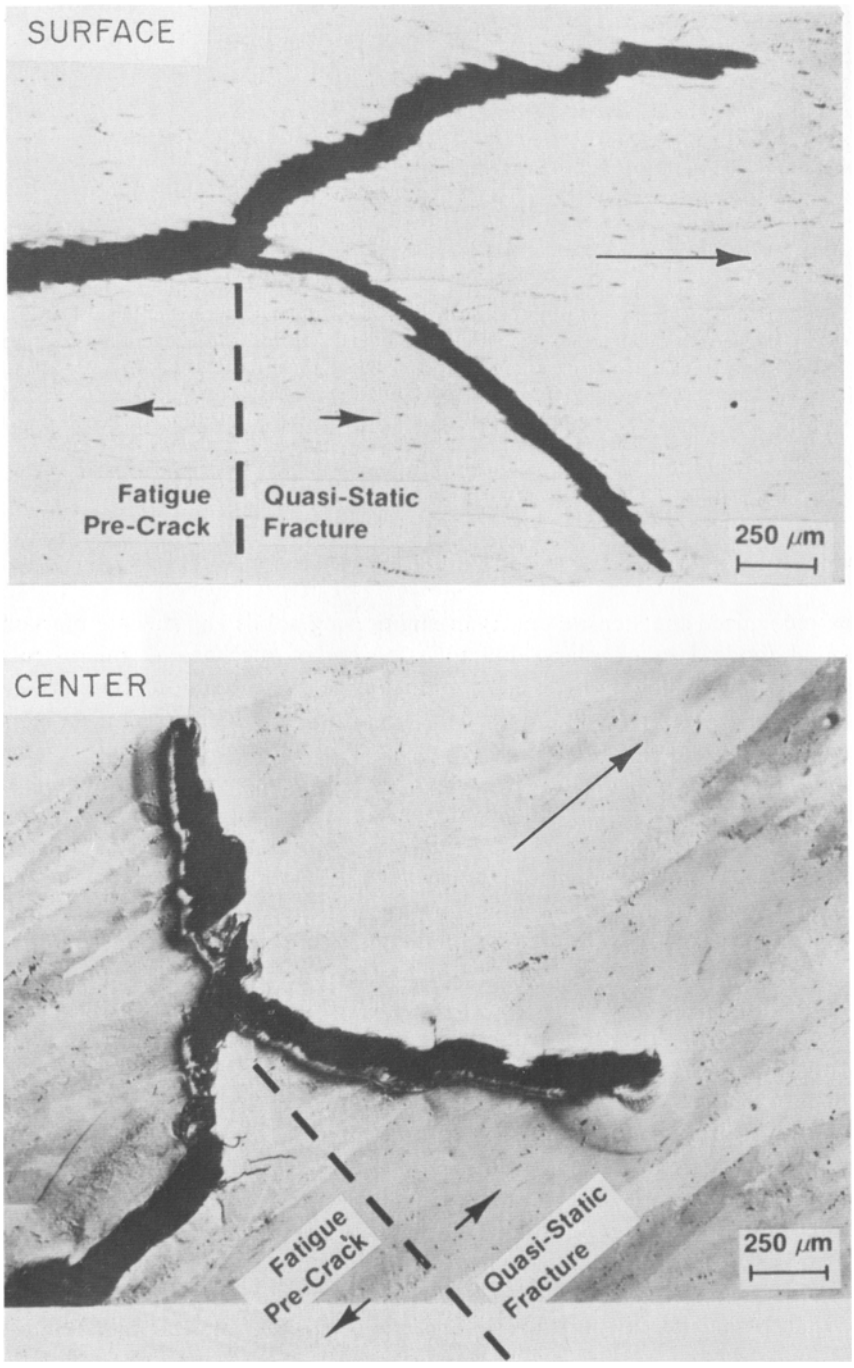

Figure 1(a). Crack branching during quasi-static fracture as observed on the surface and mid-thickness sections of a 12.74 mm thick compact specimen of an A1-2.9 Cu-2.1 Li-0.12 Zr alloy [14]. Larger arrows indicate the nominal mode I crack growth direction.

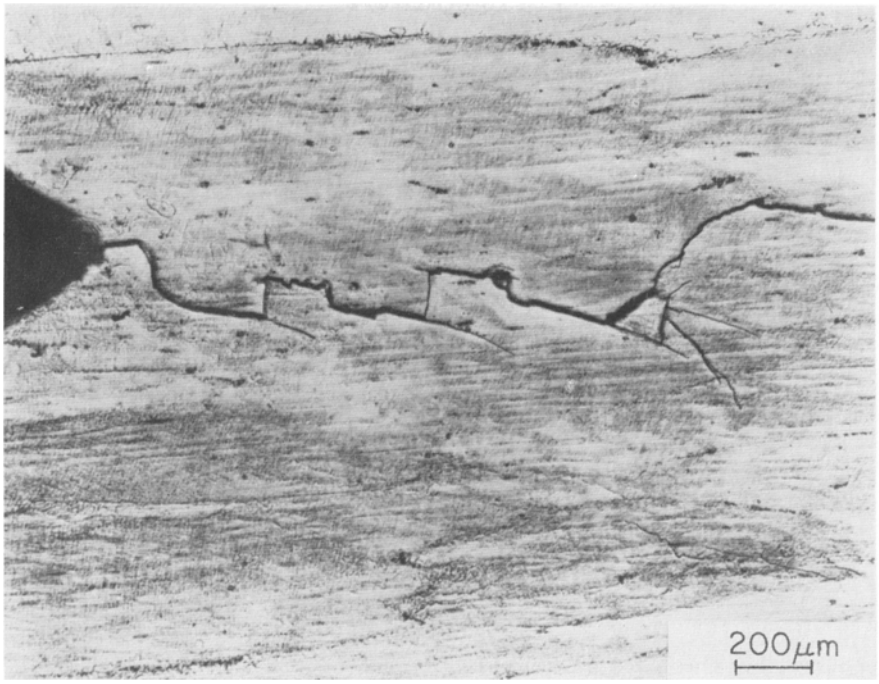

Figure 1(b). Branched fatigue crack growth in an underaged temper of the same alloy [15].

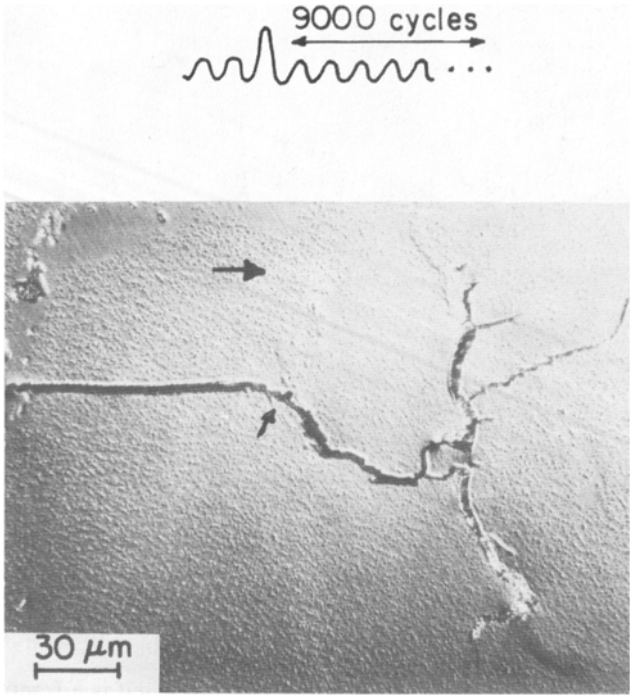

Figure 1(c). Kinking of a fatigue crack (denoted by the smaller arrow) due to the application of an 80 percent overload at baseline $\Delta K_I = 7.5$ mPa$\sqrt{m}$ and subsequent development of a fork when the crack-tip intersects a grain boundary in aluminum alloy 2020-T651 [16]. The larger arrow indicates the nominal mode I crack growth direction.

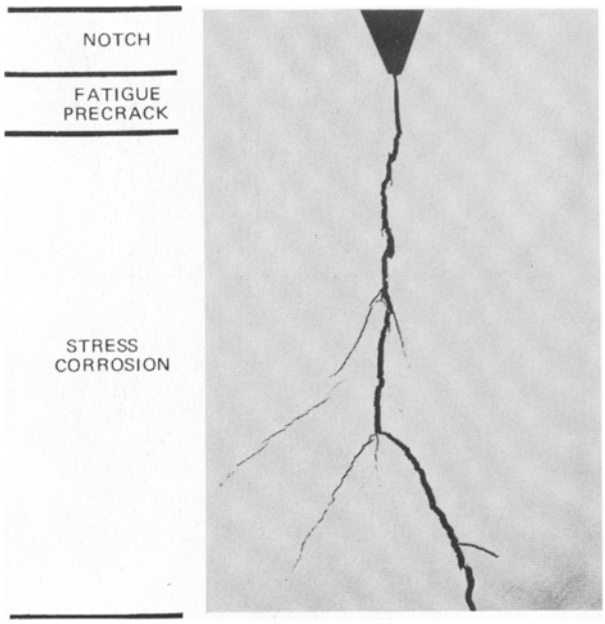

Figure 1(d). Stress corrosion crack branching in 9Ni-4 Co-0.45C martensitic steel [17].

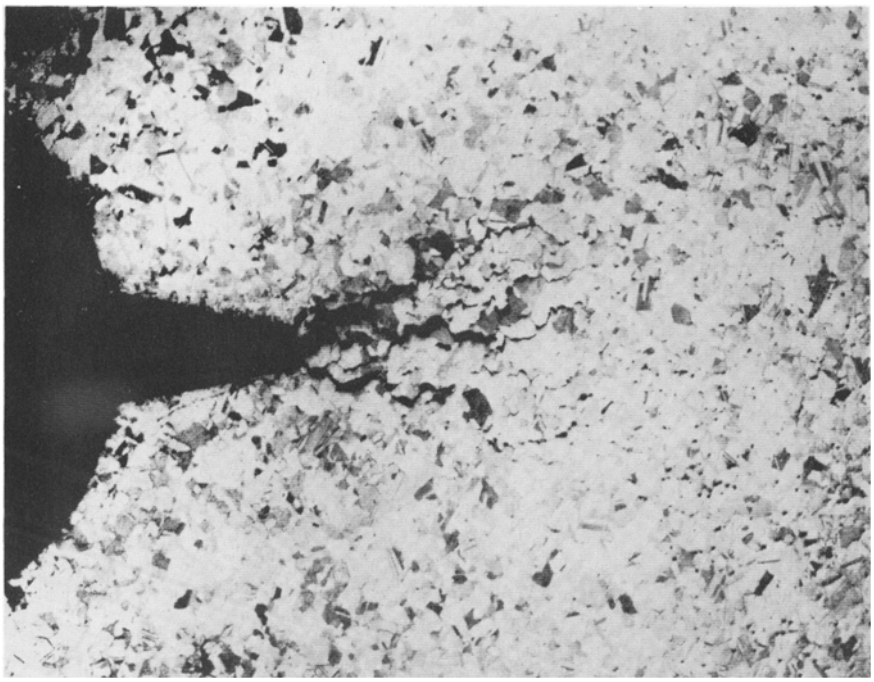

Figure 1(e). Creep crack growth in copper [18].

zone of dominance of the k_1 and k_2 singular fields which itself is a fraction of the kink or fork length. In situations where the crack tip plasticity develops over a substantial fraction of the kink or fork length, the relevance of the elastic k_1 and k_2 characterization of the near-tip fields becomes questionable. For example, at elevated temperatures, which are

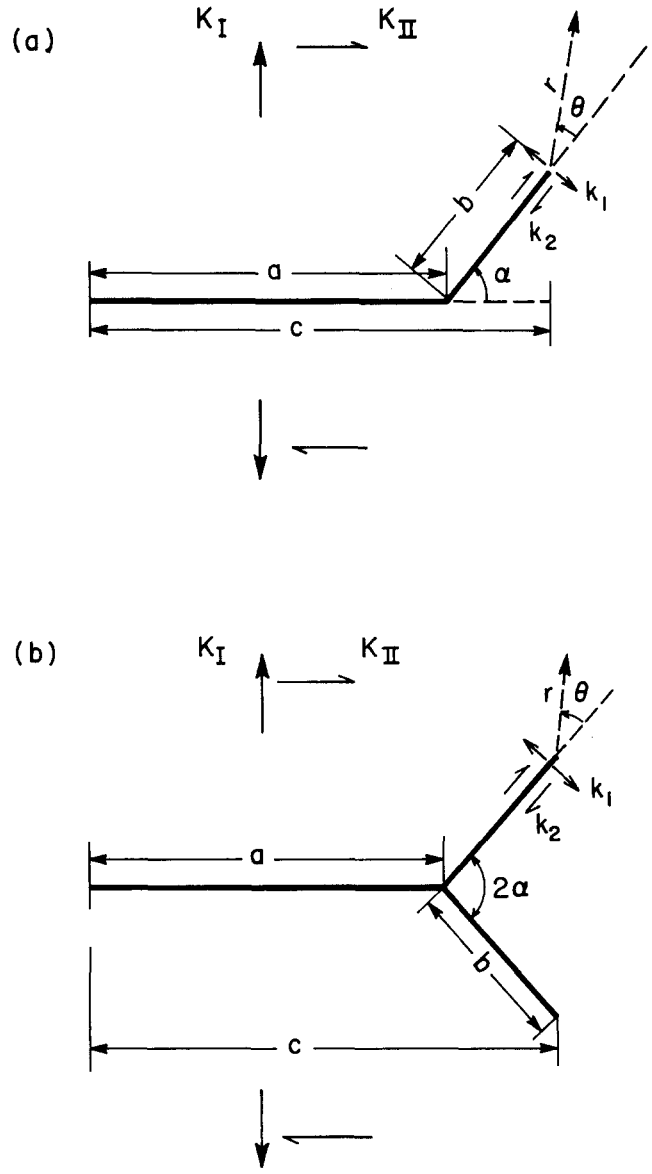

Figure 2. Schematic showing (a) kinked and (b) forked cracks and the associated nomenclature.

typical of service conditions, crack tip plasticity can develop over a distance which is comparable to the length of the kink or fork even in nominally brittle materials like ceramics. The presence of plasticity could limit the usefulness of elastic analysis for rationalizing toughening induced by crack deflection (e.g. [13]). In this connection, we note that the plastic zone size under mixed mode loading is substantially larger than that associated with pure mode I loading at the same effective amplitude of loading [19,20]. Thus plasticity effects could be more important for branched cracks.

In this paper we outline a procedure for the determination of plastic near-tip stress and deformation fields under plane strain and small scale yielding conditions for kinked and forked cracks. This method utilizes the existing stress intensity factor solutions [5–8] for kinked and forked cracks and the universal mixed-mode plastic near-tip fields [19–20] to determine the stress and deformation states in the immediate vicinity of the tip of the

kinked or forked crack. The near-tip fields are characterized by an amplitude and a mixity parameter. The procedure allows us to examine the influence of plasticity and strain hardening characteristics on the local stress and deformation state. We discuss the possible beneficial effects of crack tip plasticity on fracture toughness and crack growth resistance for branched cracks.

2. Stress intensity factor solutions for kinked and forked elastic cracks

We give a brief review of some of the salient features of two-dimensional elastic solutions for branched cracks upon which our further developments are predicated. Figure 2 shows an idealized line crack containing a kink inclined at an angle α from the main crack plane and a symmetrically forked crack with an included angle of 2α. Several investigators have suggested that the stress intensity factors at the tip of a kinked crack can be calculated to the first order from stresses that exist in the line of the pupative kink [9,10]. Let K_{I} and K_{II} denote the mode I and mode II stress intensity factors of the main crack in the absence of the kink or the fork. The local tensile (mode I) and sliding (mode II) stress intensity factors k_1 and k_2, for the infinitesimal kink ($b/a \to 0$) can be expressed in the form (see [6,9,10])

$$k_1 = a_{11}(\alpha)K_{\mathrm{I}} + a_{12}(\alpha)K_{\mathrm{II}}$$
$$k_2 = a_{21}(\alpha)K_{\mathrm{I}} + a_{22}(\alpha)K_{\mathrm{II}}. \tag{2.1}$$

To a first order approximation in α, the dimensionless factors for the infinitesimal kink are given by (see [9,10])

$$a_{11}(\alpha) = \frac{1}{4}\left[3\cos\left(\frac{\alpha}{2}\right) + \cos\left(\frac{3\alpha}{2}\right)\right]$$
$$a_{12}(\alpha) = -\frac{3}{4}\left[\sin\left(\frac{\alpha}{2}\right) + \sin\left(\frac{3\alpha}{2}\right)\right]$$
$$a_{21}(\alpha) = \frac{1}{4}\left[\sin\left(\frac{\alpha}{2}\right) + \sin\left(\frac{3\alpha}{2}\right)\right]$$
$$a_{22}(\alpha) = \frac{1}{4}\left[\cos\left(\frac{\alpha}{2}\right) + 3\cos\left(\frac{3\alpha}{2}\right)\right]. \tag{2.2}$$

Results (2.1) and (2.2) have been corroborated by a number of independent studies. In particular, we mention Lo's exact formulation of the elastic crack problem, which provides a unified method for solving the infinitesimal and finite kinked and forked cracks [8]. Lo obtained his solutions by treating the crack problem as a continuous distribution of dislocations. For a crack containing an infinitesimally small kink at its tip($b/a \to 0$ in Fig. 2a), Lo's solution and those of Bilby, Cardew and Howard [6] and Palaniswamy and Knauss [2] are in good agreement. Cotterell and Rice [9] have noted that in the case of an infinitesimal kink, the approximate solutions (2.1) and (2.2) are within 5 percent of the above consensus solutions for large angles of deviation (up to 40 degrees) from the plane of the main crack. In the case of a finite size kink and fork, the solutions of Lo [8] and Kitagawa, Yuuki and Ohira [5] are in good agreement. Some disagreement between the solutions in [5,8] and Bilby et al.'s [6] forked crack solutions for $b/a = 0.025$ have been noted.

The variation of the angular functions $a_{ij}(\alpha)$ defined by (2.2) with respect to kink angle α is shown in Fig. 3a for an infinitesimal kink ($b/a \leqslant 0.01$) ahead of a main crack. These results are taken from Bilby et al. [6]. Hereafter we direct our discussion to a macroscopic branched crack in a plate whose dimensions are large compared to the size of the crack; the plate is subject to remote tension only. The normalized stress intensity factor solutions

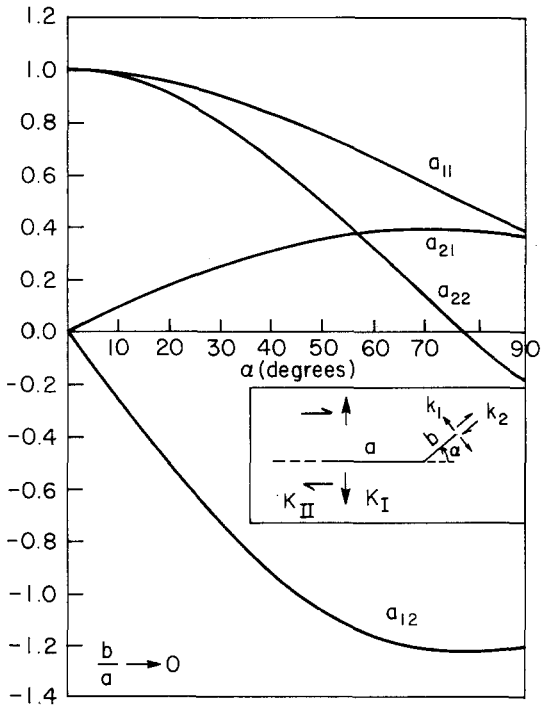

Figure 3(a). Variation of the angular functions a_{ij} with the kink angle α for $b/a \to 0$ [6].

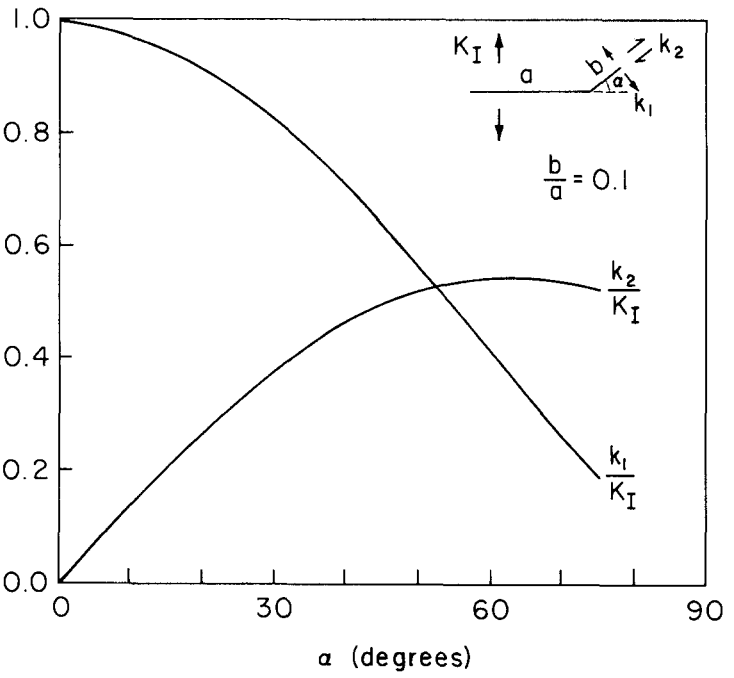

Figure 3(b). Variation of normalized k_1 and k_2 with kink angle α for $b/a = 0.1$ [5].

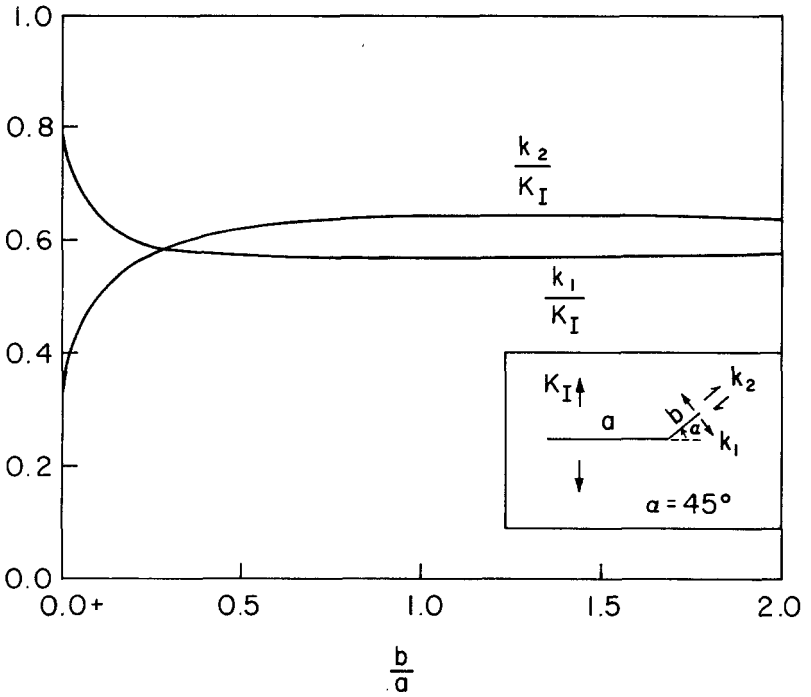

Figure 3(c). Variation of normalized k_1 and k_2 with b/a for a kink angle $\alpha = 45$ degrees [5,8].

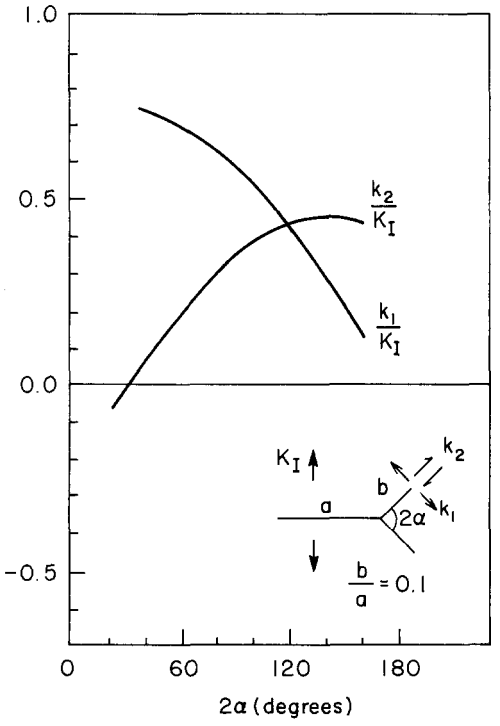

Figure 4(a). Variation of normalized k_1 and k_2 with the included fork angle 2α for $b/a = 0.1$ [5].

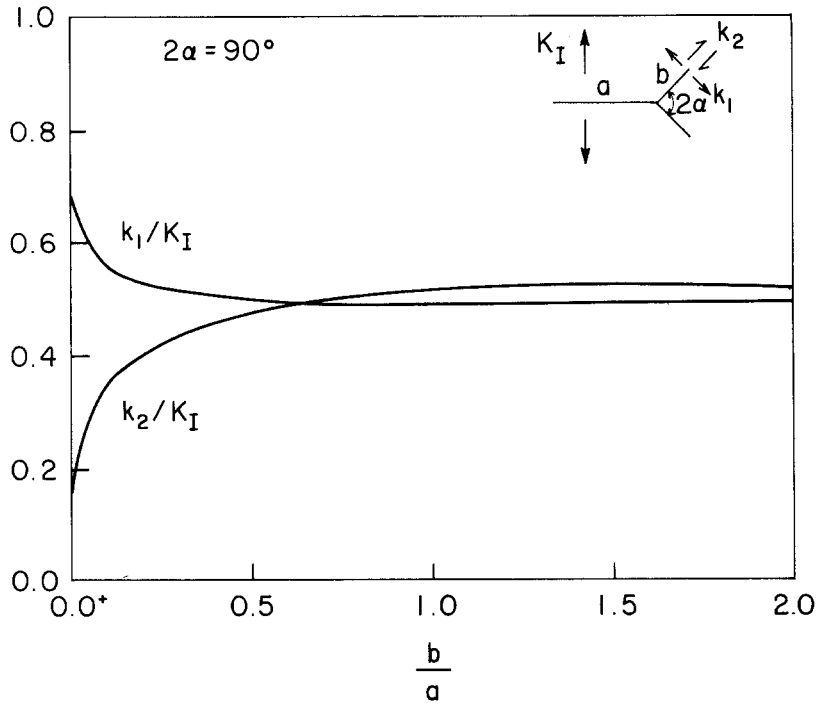

Figure 4(b). Variation of normalized k_1 and k_2 with b/a for a fork angle $2\alpha = 90$ degrees [5,8].

for the finite kinked crack ($b/a = 0.1$) are shown in Fig. 3b. As discussed previously the nominal stress intensity factor K_I is based upon the projected length c. For a kink angle of 45 degrees the stress intensity factors as a function of the kink length (b/a) are shown in Fig. 3c. The latter two figures were put together using results from Kitagawa et al. [5] and Lo [8].

Figure 4a shows the dependence of the stress intensity factors k_1 and k_2 on the included angle 2α for the finite forked crack with relative fork length $b/a = 0.1$. The dependence of k_1 and k_2 on the relative fork length for an included angle of $2\alpha = 90$ degrees is shown in Fig. 4b. Both figures were put together using results from Lo [8] and Kitagawa et al. [5]. The latter noted that k_2 vanishes at an angle α of 16 degrees for $b/a = 0.1$, as indicated in Fig. 4a. A similar result was observed by Bilby et al. [6] who found that k_2 vanishes at α of 18 degrees for $b/a = 0.025$. It may be noted that the normalized values of k_1 and k_2 in Figs. 3c and 4b do not vary with b/a for b/a greater than about 0.5. This is in accord with the known result that the kinked and forked crack solutions for b/a greater than 0.5 approach those for a crack inclined at an angle of β radians ($\beta = (\pi/2) - \alpha$) to a remote tension field.

3. Plastic near-tip fields under mixed mode loading in plane strain

3.1. Characterization of plastic near-tip fields

We consider a Ramberg-Osgood material where the uniaxial strain ϵ is related to the uniaxial stress σ by

$$\frac{\epsilon}{\epsilon_0} = \frac{\sigma}{\sigma_0} + \alpha_0 \left(\frac{\sigma}{\sigma_0}\right)^n \tag{3.1}$$

where σ_0 is the yield stress, $\epsilon_0 = \sigma_0/E$ is the yield strain, E is the Young's modulus, α_0 is a material constant and n is the strain hardening exponent. For the dominant singularity of the near-field, the elastic strains are negligible compared to the plastic strain and hence only the plastic part of the stress-strain relation enters in the analysis of the plastic near-tip fields.

With reference to crack-tip polar coordinates (r, θ) the dominant singularity governing the behavior of the stresses, strains and displacements at the crack tip has the form [19,20].

$$\sigma_{ij} = \sigma_0 K^p r^{-1/(n+1)} \tilde{\sigma}_{ij}(\theta;\ M^p,\ n)$$

$$\epsilon^p_{ij} = \frac{\alpha_0}{E}(K^p)^n r^{-n/(n+1)} \tilde{\epsilon}_{ij}(\theta;\ M^p,\ n)$$

$$u_i = \frac{\alpha_0}{E}(K^p)^n r^{1/(n+1)} \tilde{u}_i(\theta;\ M^p,\ n) \tag{3.2}$$

where the θ-variations of the dimensionless functions $\tilde{\sigma}_{ij}$, $\tilde{\epsilon}_{ij}$, $\tilde{u}_i$ depend on the near-field mixity parameter M^p and n. The amplitude of the singular fields is K^p and this is given precise meaning by setting the maximum value of the θ-variation of the effective stress, $\tilde{\sigma}_e = [(3/2)\tilde{s}_{ij}\tilde{s}_{ij}]^{1/2}$ to unity, where $\tilde{s}_{ij} = \tilde{\sigma}_{ij} - (\tilde{\sigma}_{kk}/3)\delta_{ij}$.

The plastic mixity parameter M^p is introduced in (3.2) to identify each possible set of θ-variations of stresses and strains. One convenient way of identification is the relative composition of mode I and mode II conditions directly ahead of the tip given by the ratio of the tensile stress to shear stress,

$$M^p = \frac{2}{\pi}\tan^{-1}\left|\lim_{r\to 0}\frac{\sigma_{\theta\theta}(r,\ \theta=0)}{\sigma_{r\theta}(r,\ \theta=0)}\right|$$

$$= \frac{2}{\pi}\tan^{-1}\left|\frac{\tilde{\sigma}_{\theta\theta}(\theta=0;\ M^p,\ n)}{\tilde{\sigma}_{r\theta}(\theta=0;\ M^p,\ n)}\right|. \tag{3.3}$$

With this definition M^p ranges from 0 to 1, with $M^p = 0$ for pure mode II and $M^p = 1$ for pure mode I conditions in the plastic fields. Thus the two parameters K^p and M^p completely identify the plastic near-tip fields for a given value of n. The θ-variations of the universal dimensionless functions $\tilde{\sigma}_{ij}$, $\tilde{\epsilon}_{ij}$ and the effective stress $\tilde{\sigma}_e$ are shown in Figs. 5 and 6 for $n = 3$ and 13 respectively; the four cases are arranged in order of increasing asymmetry.

What is significant about these fields is the dramatic drop in the tensile stress $\tilde{\sigma}_{\theta\theta}$ and the stress triaxiality as the conditions change from mode I to mode II. This is a plasticity effect which is not observed for the elastic $(n = 1)$ mixed mode solutions. A deviation from mode I conditions also changes the plastic strain distribution ahead of the crack. Furthermore, it is worth mentioning that at the same level of applied load as measured by J, the mode II plastic zone is about 5 times larger than the mode I plastic zone [19,20]. The implications of plasticity effects on fracture toughness and crack growth resistance under mixed mode loading are examined in Section 5.

In pure mode I or pure mode II, the plastic stress intensity factor K^p can be related to the remote loading through the path-independent J-integral [21]. Indeed the amplitude of the well-known Hutchinson-Rice-Rosengren (HRR) singularity fields is given by J [22,23]. Under mixed mode loading, K^p can also be expressed in terms of J, but the expression depends implicitly on the additional parameter M^p,

$$J = \frac{\alpha_0^2}{E} I_n(M^p)(K^p)^{n+1}. \tag{3.4}$$

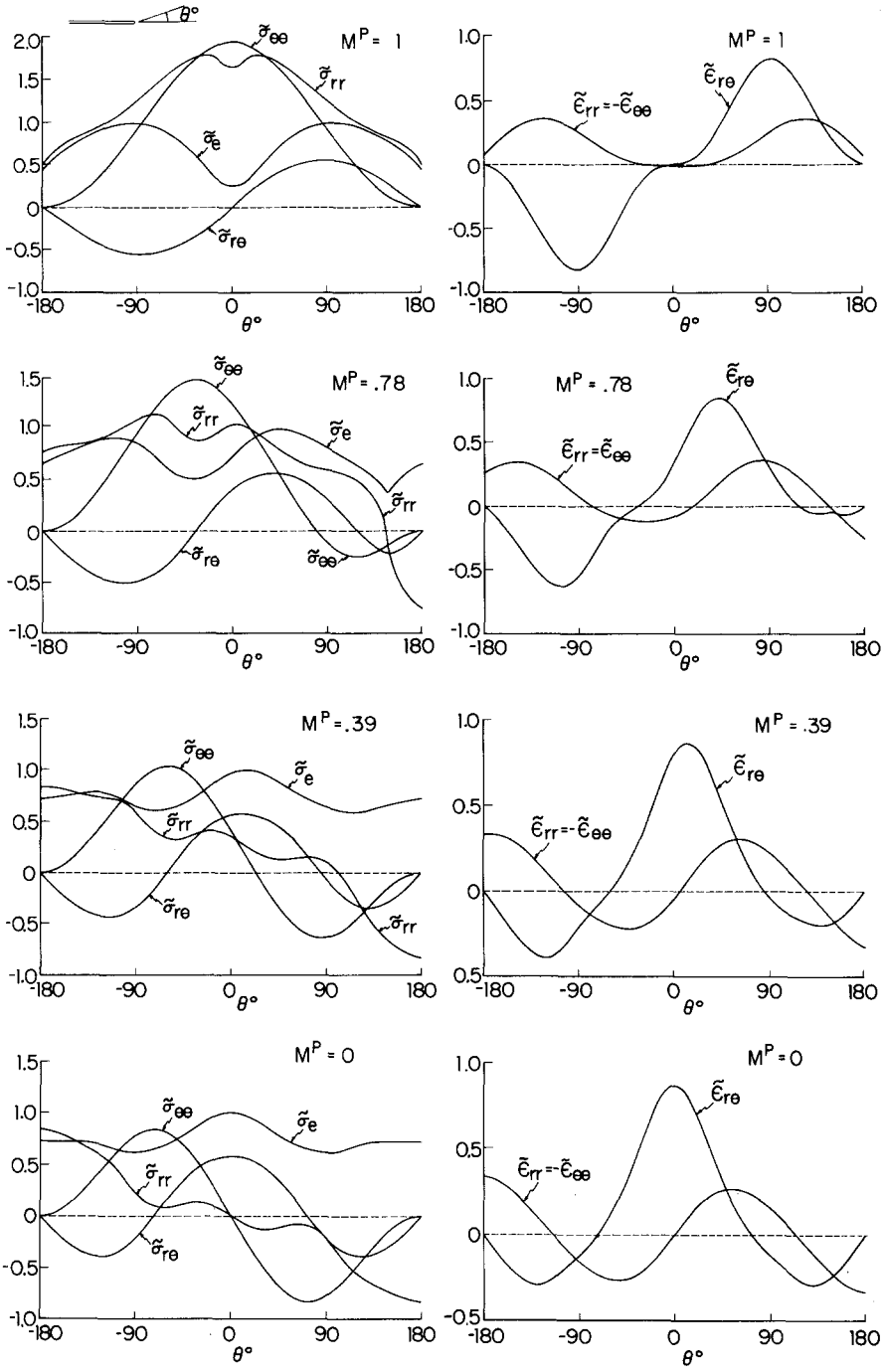

Figure 5. Circumferential variations of stresses and strains at the tip of a crack for $n = 3$ [19,20].

The dependence of the numerical constant I_n on M^p for a wide range of hardening behaviour is shown in Fig. 7. Contrary to some initial hopes the additional relationship required to connect K^p and M^p to remote loading could not be found from the known conservation integrals [24,25]. Thus the connection of the plastic singular fields characterized by K^p and M^p to the remote loads requires a full field analysis. This full field analysis has been carried out for small scale yielding [19,20].

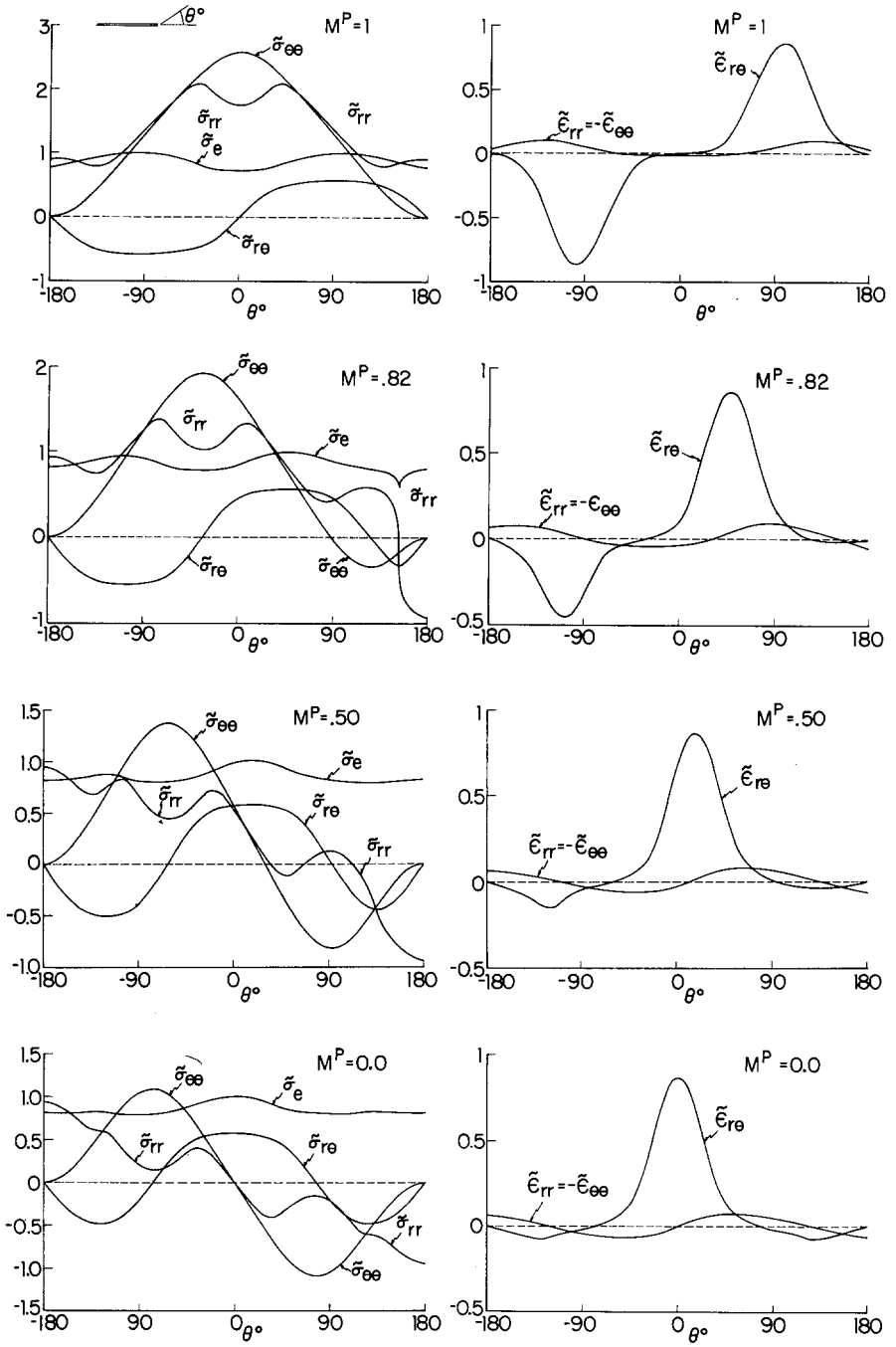

Figure 6. Circumferential variations of stresses and strains at the tip of a crack for $n = 13$ [19,20].

3.2. *Relating K^p and M^p to k_1 and k_2: the small scale yielding problem*

At distances large compared to the plastic zone but still small compared to b (the length of the kink or fork) the elastic singularity dominates the stress (and strain) distributions, i.e.,

$$\sigma_{ij} = (2\pi r)^{-1/2}\left[k_1\sigma_{ij}^{\mathrm{I}}(\theta) + k_2\sigma_{ij}^{\mathrm{II}}(\theta)\right] \tag{3.5}$$

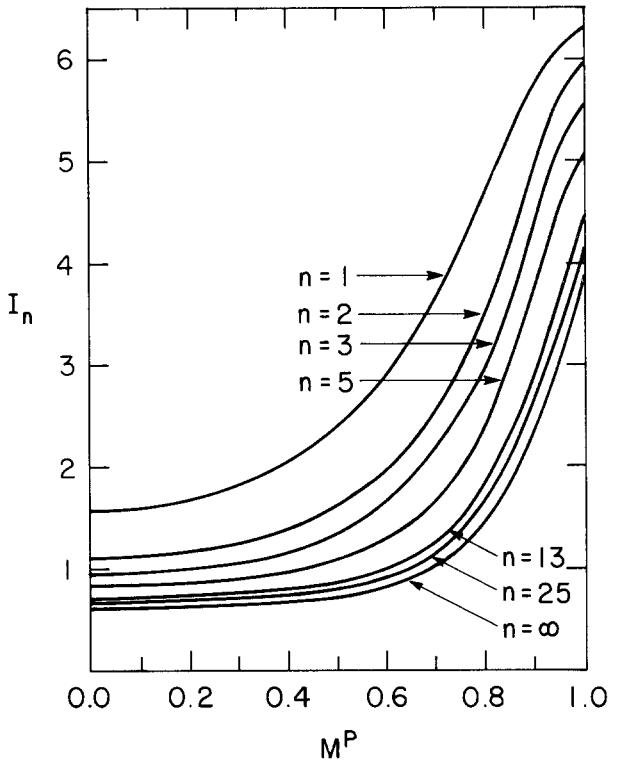

Figure 7. Relationship between I_n and M^p under plane strain conditions [19,20].

where k_1 and k_2 are the elastic stress intensity factors appropriate to the kink or fork, r and θ are the polar coordinates indicated in Fig. 2 and σ_{ij}^{I} and $\sigma_{ij}^{\mathrm{II}}$ are the well known dimensionless angular functions.

Under small scale yielding, and for plane strain conditions,

$$J = \frac{1-\nu^2}{E}\left(k_1^2 + k_2^2\right) \tag{3.6}$$

where ν is Poisson's ratio. Thus J may be thought of as the effective amplitude of the elastic singularity. We emphasize that (3.6) may be interpreted as the energy released by the body (per unit area of crack advance) only if the crack advances in its own plane. This will be further elaborated upon in Section 5. Following the approach taken in Section 3.1, the relative composition of elastic mode I and II conditions in the region dominated by (3.5) can be characterized by the elastic mixity parameter M^e defined by

$$M^e = \frac{2}{\pi}\tan^{-1}\left|\frac{k_1\sigma_{\theta\theta}^{\mathrm{I}}(\theta=0)}{k_2\sigma_{r\theta}^{\mathrm{II}}(\theta=0)}\right| = \frac{2}{\pi}\tan^{-1}\left|\frac{k_1}{k_2}\right|. \tag{3.7}$$

Thus $M^e = 0$ for pure mode II and $M^e = 1$ for pure mode I conditions in the zone governed by the elastic singular fields. To illustrate the definition (3.7), we consider a "main" mode I crack subject to remote tensile loading and containing a small kink ($b/a \leqslant 0.01$) deflected from the "main" crack plane by an angle α. Using the result (2.2), the elastic mixity parameter M^e is given by

$$M^e = \frac{2}{\pi}\tan^{-1}\left[\cot\left(\frac{\alpha}{2}\right)\right]. \tag{3.8}$$

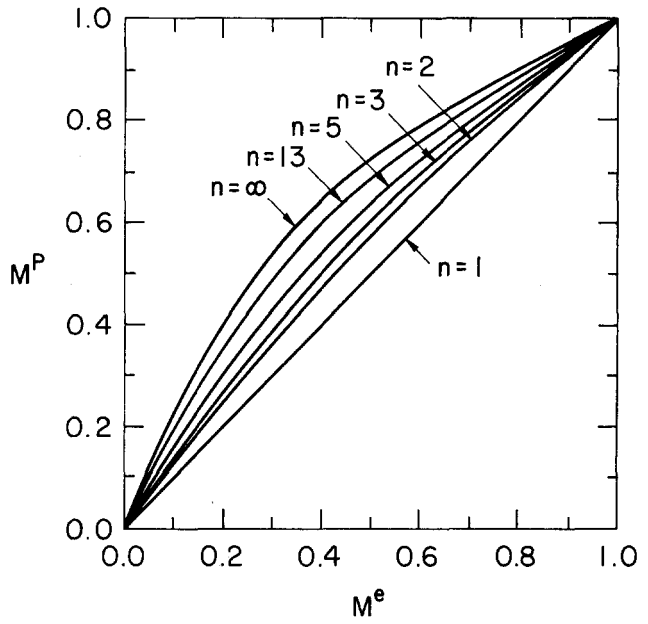

Figure 8. Near-field mixity parameter M^p versus far-field mixity parameter M^e for small scale yielding in plane strain [19,20].

In pure mode I (or pure mode II), the plastic stress intensity factor K^p can be expressed directly in terms of the corresponding elastic stress intensity factor k_1 (or k_2) by exploiting the path-independence of J. Under mixed mode loading and small scale yielding conditions, we use (3.4) and (3.6) to write K^p in terms of k_1 and k_2; the resulting expression depends implicitly on M^p, that is,

$$J = \frac{1-\nu^2}{E}\left(k_1^2 + k_2^2\right) = \frac{\alpha_0^2}{E} I_n(M^p)(K^p)^{n+1}. \tag{3.9}$$

A complete specification of the plastic near-tip fields in terms of k_1 and k_2 (or equivalently J and M^e) requires that the relationship between M^e and M^p be known. As already noted, the known conservation integrals did not provide this additional relationship. To date we are unaware of any method which directly connects the plastic fields (3.2) to the elastic fields (3.5) without an analysis of the elastic-plastic fields. Nevertheless for use in later discussions, a specific result will be stated.

What has come to be referred to as the J-integral is actually the first component of the vector of translational conservation integrals [24,25], i.e. $J \equiv J_1$. The second integral, J_2, is not path-independent in the sense of the J-integral and does not have an analogous energetic force interpretation [25]. For a contour which begins on one traction-free crack surface, passes along the elastic fields (3.5) and ends on the other crack surface, J_2 has the value

$$J_2 = \frac{-2(1-\nu^2)}{E} k_1 k_2. \tag{3.10}$$ *

We observe that J_2 vanishes when either k_1 or k_2 vanishes and J_2 is not a positive scalar quantity with respect to k_1 and k_2. In general J_2 does not have a physical interpretation in terms of the energy released by crack advance and does not appear to provide useful additional information for the analysis of mixed mode crack problems.

* The expression given in [19,20] contains a typographical error and is correct only for $\nu = 0.5$.

To determine the relationship between M^e and M^p a full field finite element analysis of the small scale yielding problem has been carried out in [19,20]. This relationship for the complete range of mixities and several values of n is shown in Fig. 8. Thus K^p and M^p are now known in terms of k_1 and k_2 and the plastic near-tip fields can be regarded as completely determined for small scale yielding. Plastic zone size and shapes for four values of M^e ranging from pure mode I ($M^e = 1$) to pure mode II ($M^e = 0$) are given in [19,20].

4. Plastic near-tip fields for kinked and forked cracks

The stress and deformation fields for kinked and forked cracks are determined for plane strain and small scale yielding conditions using the following procedure. With the known stress intensity factor solutions appropriate to the kinked or forked crack, the elastic mixity parameter M^e is determined according to (3.7). For small kinks ($b/a \leqslant 0.01$), M^e is given explicitly by (3.8) and for the other cases of branched cracks M^e is graphically determined by using the curves in Figs. 3 and 4. (For the case of an infinite plate containing a crack inclined at an angle β to a remote tension field, the elastic solution leads to $M^e = (2/\pi)\beta$.) Under small scale yielding, the relationship between M^e and M^p is known (Fig. 8) for essentially the complete range of the strain hardening coefficient n. As discussed in Section 3.1, for a known hardening behavior, a given value of M^p (determined from Fig. 8) defines a unique angular variation of plastic near-field stresses and strains (four such angular variations are shown in Figs. 5 and 6). Thus, for a given angle of kink or fork, α, and strain hardening exponent n, the specification of M^e and therefore of M^p (using Fig. 8) determines the angular distribution of the plastic near-tip stress and strain fields. The amplitude of the near-tip fields, namely J or K^p, is determined from (3.9).

We consider a main crack subject to remote tension; a kink emanates at an angle α from the plane of the main crack. Directing our attention to the short kink ($b/a \leqslant 0.01$), the influence of kink angle α on the dimensionless stresses $\tilde{\sigma}_{ij}$, strains $\tilde{\epsilon}_{ij}$, and the effective stress $\tilde{\sigma}_e$ directly ahead of the crack tip (i.e., $\theta = 0$), is shown in Figs. 9a and 9b for $n = 3$. An increase in the angle of branching, away from the main crack, leads to a reduction in the normalized tensile and radial stresses, ($\tilde{\sigma}_{\theta\theta}$ and $\tilde{\sigma}_{rr}$), and an increase in the shear and effective stress components, ($\tilde{\sigma}_{r\theta}$ and $\tilde{\sigma}_e$), ahead of the kink (Fig. 9a). The latter behavior also causes an enhancement of the strains in the plane of the kink (Fig. 9b). As the length of the kink increases, further changes take place in the stress and strain fields ahead of the kink. Figure 10 shows the variation of $\tilde{\sigma}_{\theta\theta}$ (ahead of the kink) with the relative kink length (b/a) for $n = 3$. The dimensionless tensile stress $\tilde{\sigma}_{\theta\theta}$ decreases initially with the self-similar growth of the incipient kink. As the size of the kink becomes comparable to that of the main crack, $\tilde{\sigma}_{\theta\theta}$ approaches the value for a crack inclined at an angle β to the remote tensile field. The plastic strains $\tilde{\epsilon}_{ij}$ increase as b/a increases; at large kink length, $b/a \geqslant 0.5$, the strain fields approach the distributions for the crack inclined at an angle β to the remote tensile field.

The dimensionless stresses of the elastic singularity, (see (3.5)), depend only on the circumferential angle θ. However, the angular functions ($\tilde{\sigma}_{ij}$, $\tilde{\epsilon}_{ij}$) of the plastic near-tip fields depend on θ as well as on the strain hardening coefficient n and on M^p. For the short kink ($b/a \to 0$) the variation of the dimensionless tensile stress $\tilde{\sigma}_{\theta\theta}$ (at $\theta = 0$) with α for three values of n ($n = 1, 3, 13$) is plotted in Fig. 11. It is apparent that the reduction in the normalized tensile and radial stresses in the plane of the crack tip becomes more pronounced as n increases. The $n = 13$ curve is indicative of the behavior for low hardening and non-hardening materials since the plastic near-tip fields for $n = 13$ and $n \to \infty$ differ negligibly (under small scale yielding). A similar plot of the dimensionless

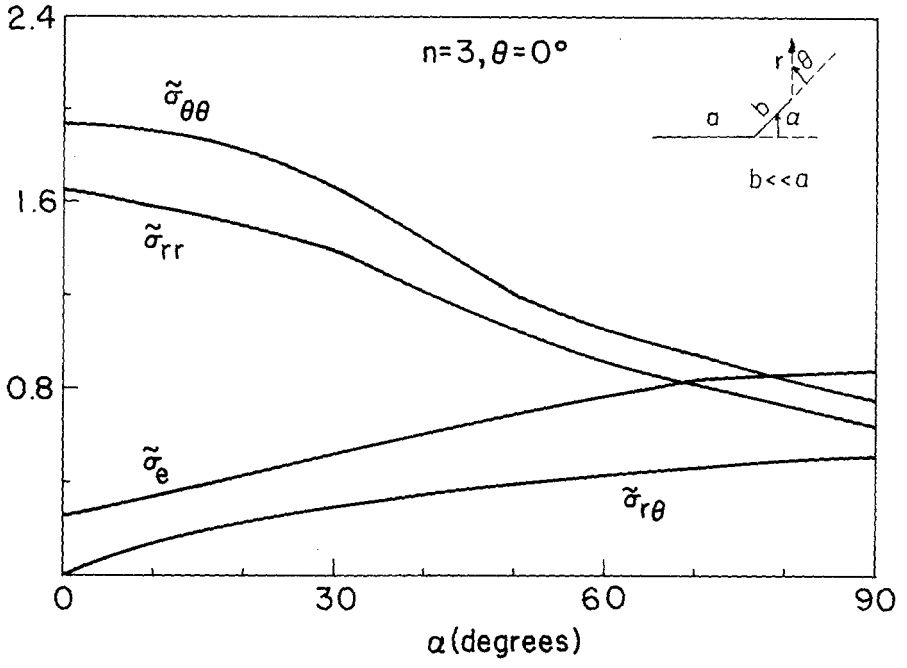

Figure 9(a). Variation of the stress components $\tilde{\sigma}_{ij}$ and $\tilde{\sigma}_e$ with the kink angle α for $n = 3$ and $b \ll a$.

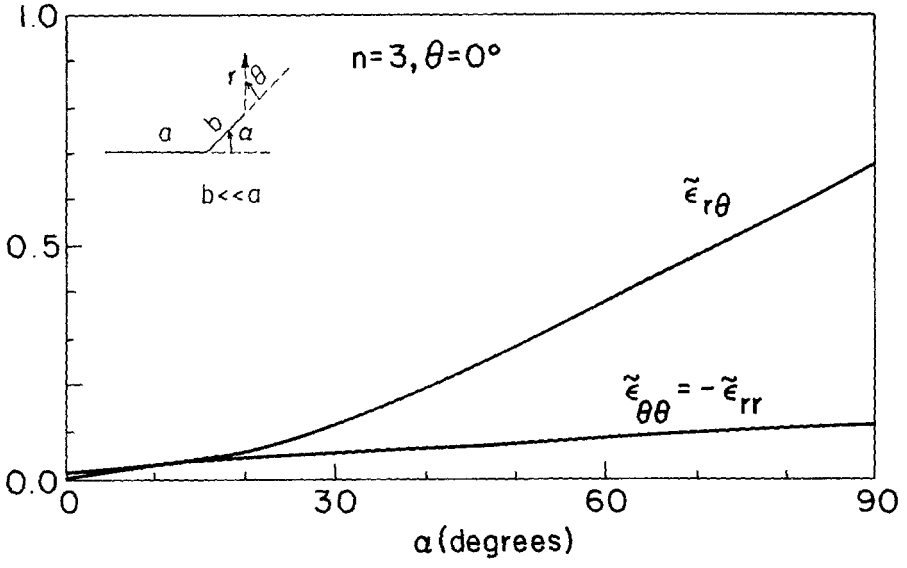

Figure 9(b). Variation of the strain components $\tilde{\epsilon}_{ij}$ with the kink angle α for $n = 3$ and $b \ll a$.

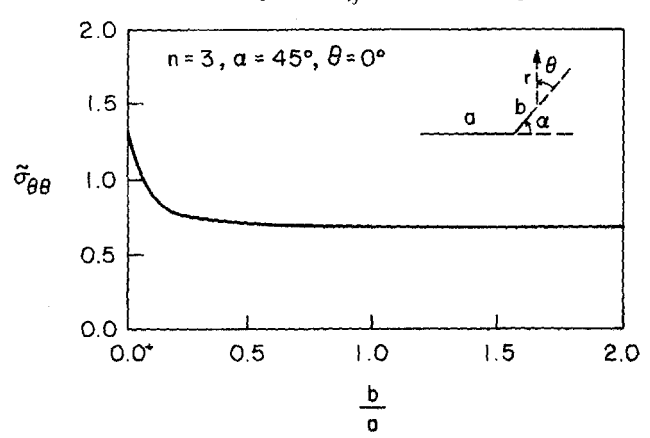

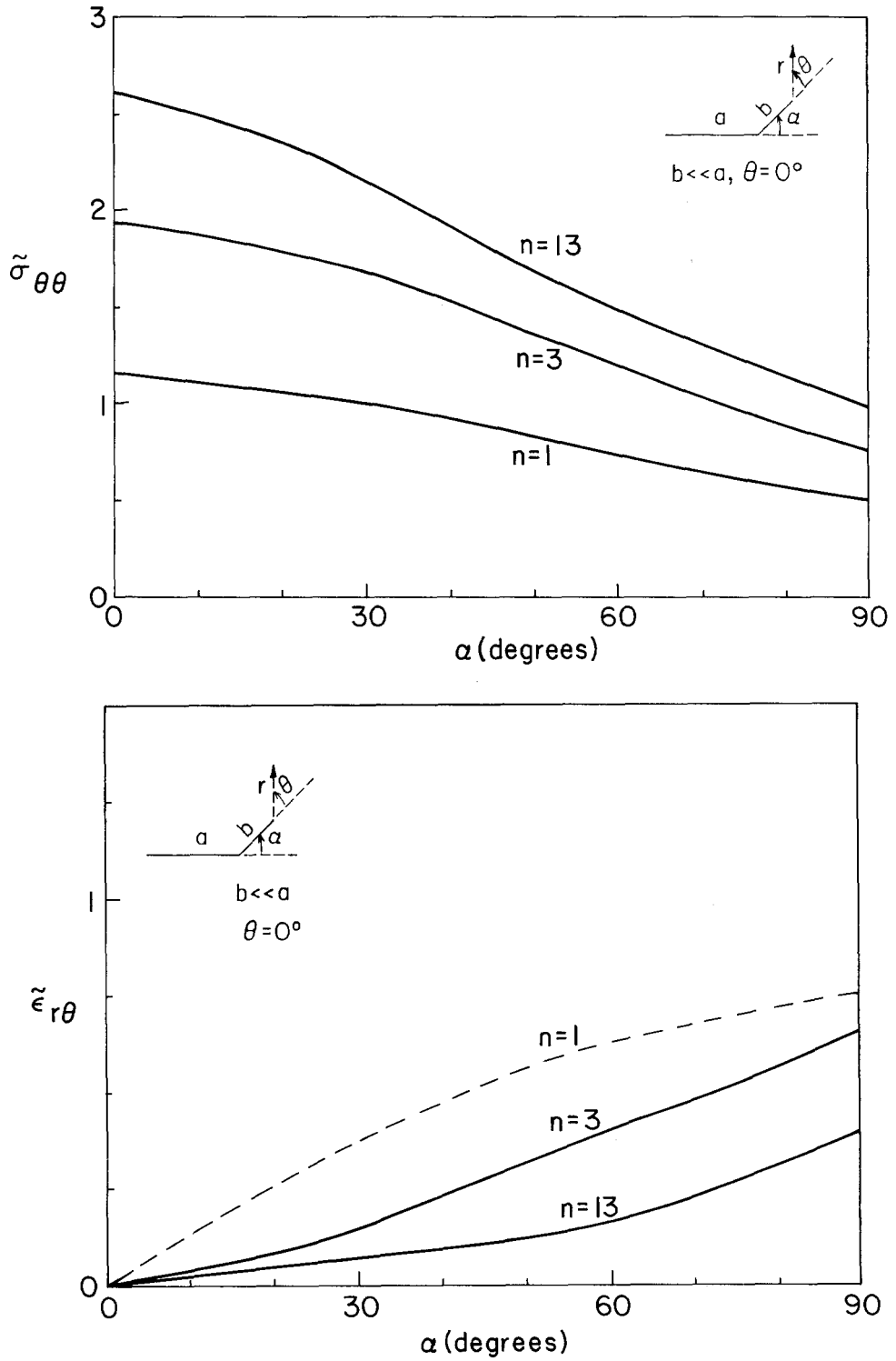

Figure 11. Variation of (a) $\tilde{\sigma}_{\theta\theta}$ and (b) $\tilde{\epsilon}_{r\theta}$ with kink angle α for an infinitesimal kink and for $n = 1$, 3 and 13.

plastic shear strain $\tilde{\epsilon}_{r\theta}$ (at $\theta = 0$) versus α is given in Fig. 11b. While the strains increase with the increase of the kink angle α, the rate of increase is considerably smaller for the $n = 13$ material.

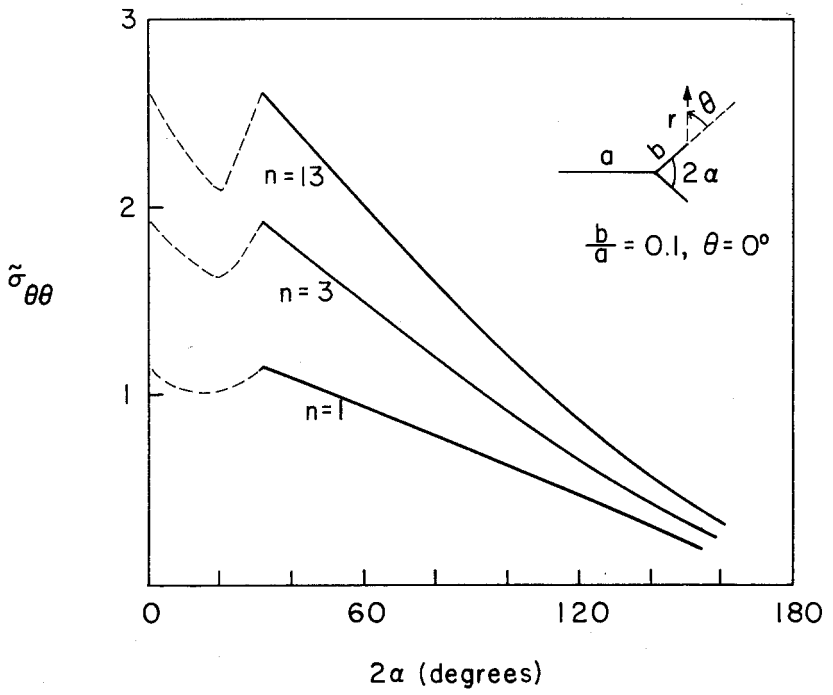

Figure 12. Variation of $\tilde{\sigma}_{\theta\theta}$ with included fork angle 2α for $b/a = 0.1$ and for $n = 1$, 3 and 13.

We also examined the near-tip fields for the symmetrically forked crack. The reduction in $\tilde{\sigma}_{\theta\theta}$ with the increase of the fork angle α (included angle is 2α) is shown in Fig. 12 for a finite size fork ($b/a = 0.1$). These curves are determined by using Figs. 4a, 5, 6, and 8. We note that the local extrema in these curves are caused by k_2 going to zero for α ranging from 34 to 38 degrees [5,6,8]. Analogous to the kinked crack case, the reduction in the magnitude of $\tilde{\sigma}_{\theta\theta}$ (at $\theta = 0$) becomes more pronounced as n increases. The variations of the other normalized stress and strain components are similar to those described for kinked cracks.

The results reported in Figs. 9 through 12 were obtained from [5,6,8,9, and 19] by reading off the plots for the pertinent solutions. For example, the plastic near-tip fields are available only at distinct values of M^p and for several values of n. Likewise some of the elastic solutions for forked cracks are given only at selected values of α and b/a. Hence we had to interpolate between distinct values to compile the required information. Consequently, the results presented in Figs. 9 through 12 are approximate and are meant to indicate trends in the changes of the plastic near-tip fields with respect to variation of the kink/fork angle and length. We emphasize that the accuracy of the results presented is only limited by the accuracy and availability of the plastic near-tip fields and the elastic solutions for branched cracks.

The above analyses do not account for deformation-induced finite geometry changes due to blunting at the tip of the branched crack. Indeed for the applications discussed, crack tip blunting would not appear to be an important factor. In the event blunting is significant, the plastic near-tip field results can be corrected accordingly. As discussed by McMeeking [26], the effects of blunting dominate over a distance of 2 to 3 times the crack tip opening displacement. Beyond this region, the small strain solutions for mixed mode fields (3.2) are expected to hold (see Hutchinson [27]).

We have presented results for plastic near-tip fields on the plane directly ahead of the kink or fork, i.e., $\theta = 0$. The procedure outlined above can be employed to obtain similar results for any value of θ.

5. Discussion

We discuss the implications of the preceding results on fracture toughness and crack growth behavior. For this purpose it is helpful to combine (3.2) and (3.4) to get the near-tip stresses and strains in the following form [20,22,23,27]:

$$\sigma_{ij} = \sigma_0 \left[\frac{J}{\alpha_0 \sigma_0 \epsilon_0 I_n r} \right]^{1/(n+1)} \tilde{\sigma}_{ij}(\theta;\, M^p,\, n)$$
$$\epsilon_{ij} = \alpha_0 \epsilon_0 \left[\frac{J}{\alpha_0 \sigma_0 \epsilon_0 I_n r} \right]^{n/(n+1)} \tilde{\epsilon}_{ij}(\theta;\, M^p,\, n). \tag{5.1}$$

At fixed values of J and radial distance r from the crack tip, the near-tip stresses and strains vary as

$$\sigma_{ij} \propto \tilde{\sigma}_{ij}(I_n)^{-1/(n+1)} = \hat{\sigma}_{ij}$$
$$\epsilon_{ij} \propto \tilde{\epsilon}_{ij}(I_n)^{-n/(n+1)} = \hat{\epsilon}_{ij} \tag{5.2}$$

where as noted previously, I_n depends on M^p and hence on the branch angle α. With the value of J and the radial distance r fixed, the mixed mode near-tip stresses and strains are directly proportional to $\hat{\sigma}_{ij}$ and $\hat{\epsilon}_{ij}$ respectively.

As discussed in the introduction there are ample experimental data which show that the development of kinks and/or forks ahead of a main crack is generally accompanied by an increase in both the fracture initiation toughness and the crack growth resistance. To develop our argument that crack tip plasticity further enhances such beneficial effects, we consider three materials containing identically sized and shaped cracks: an ideally elastic material ($n = 1$), a high hardening material ($n = 3$) and a low hardening material ($n = 13$). These cracked bodies are subject to identical remote tensile stresses which result in identical near-field loading as defined by the value of J (3.6). Let $\hat{\sigma}^{\mathrm{I}}_{\theta\theta}$ denote the normalized tensile hoop stress directly ahead of the crack ($\theta = 0$) when the branch angle α is zero. A measure of the relative change of the hoop stress ahead of the crack ($\theta = 0$) with branch angle is the ratio $\hat{\sigma}_{\theta\theta}/\hat{\sigma}^{\mathrm{I}}_{\theta\theta}$.

For the short kink ($b \ll a$) this ratio is plotted as a function of α in Fig. 13 for the ideally elastic crack ($n = 1$) and the cracks with yielded near-tip region ($n = 3$ and 13). As the branch angle increases the tensile hoop stress directly ahead of the branch falls off rapidly; furthermore the stress reduction is most pronounced for the low hardening material ($n = 13$). The variation of the hydrostatic stress with α is nearly identical to the trends seen in Fig. 13; for this reason the hydrostatic stress plots are not given. The curves in Fig. 13 in conjunction with a crack growth criterion based on the attainment of a critical value of the tensile stress certainly suggest that crack tip plasticity enhances the beneficial effects of crack branching.

A ductile crack growth criterion based on the attainment of a critical value of the tensile strain over a microstructurally-relevant distance has been proposed by several investigators. Experiments with notched bars show that the value of the tensile strain at failure decreases as the hydrostatic stress increases (e.g. [28]). These observations take on a particular significance since the hydrostatic stress level drops by a substantial amount as the near-tip conditions deviate from mode I (see Figs. 5 and 6). Under mixed mode conditions it is not obvious that crack growth should be correlated to a critical value of a single strain component. A strain measure which depends on all strain components is the effective strain defined by

$$\epsilon_e^2 = \tfrac{2}{3}\epsilon_{ij}\epsilon_{ij}. \tag{5.3}$$

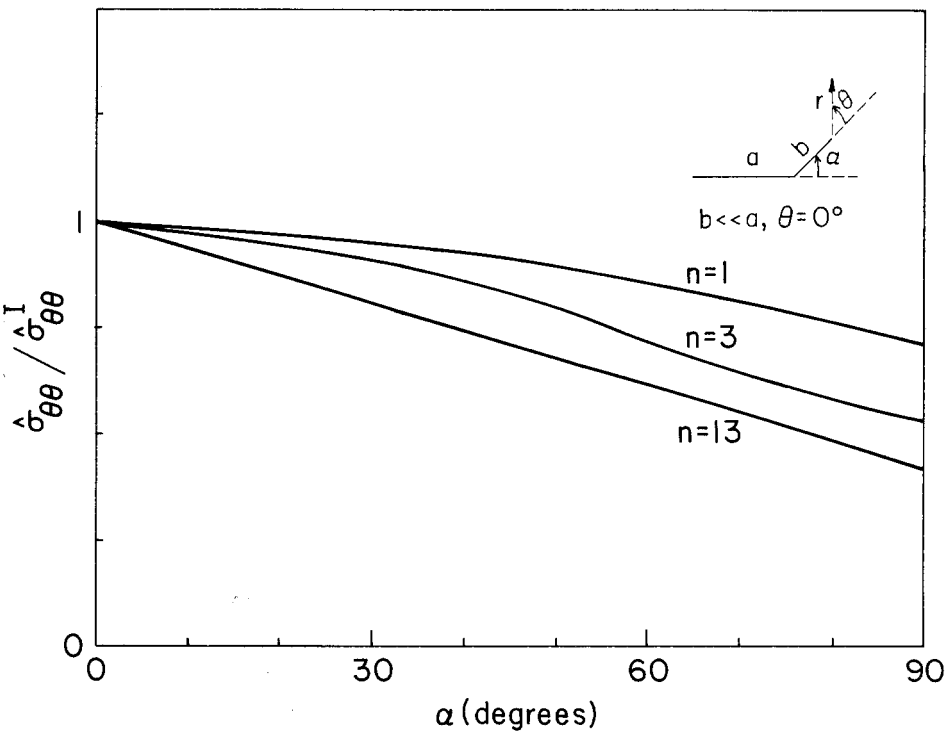

Figure 13. Reduction of the normalized tensile stress with increasing branch angle for $n = 1$, 3 and 13.

To gauge the change of ϵ_e with branch angle α at fixed values of J and radial distance r close to the crack tip, we introduce the normalized effective strain

$$\hat{\epsilon}_e = \left(\tfrac{2}{3}\tilde{\epsilon}_{ij}\tilde{\epsilon}_{ij}\right)^{1/2}(I_n)^{-n/(n+1)} \tag{5.4}$$

where $\tilde{\epsilon}_{ij}$ are the dimensionless near-tip strains in (5.1). Figure 14 shows $\hat{\epsilon}_e$ directly ahead of the branch ($\theta = 0$) increases as the branch angle increases; however at a given branch angle the strain magnitude is smaller for the low-hardening model. If the critical strain value for crack growth depends strongly on the hydrostatic stress (as experiments indicate [28]) then Figs. 13 and 14 together seem to suggest that crack tip plasticity further enhances the beneficial effects of the branching.

Recent studies of fracture behavior in Al-Li-Cu-Zr alloys reveal that the underaged tempers exhibit up to a threefold increase in fracture toughness compared to the overaged microstructures of the same material heat-treated to give comparable flow strength and strain hardening properties [14]. It appears that a major factor for such beneficial fracture properties is the development of a branched crack tip during quasi-static fracture initiation. On the basis of elastic analysis and an energy release rate criterion, one can rationalize an increase in toughness by a factor of 1.6 only. The present study suggests that the additional increase in fracture toughness can at least be partially accounted for by near-tip plasticity effects.

When a branched elastic crack advances along the plane of the branch, the energy release rate, G, under plane strain is given by

$$G = \frac{1-\nu^2}{E}\left\{k_1^2 + k_2^2\right\}. \tag{5.5}$$

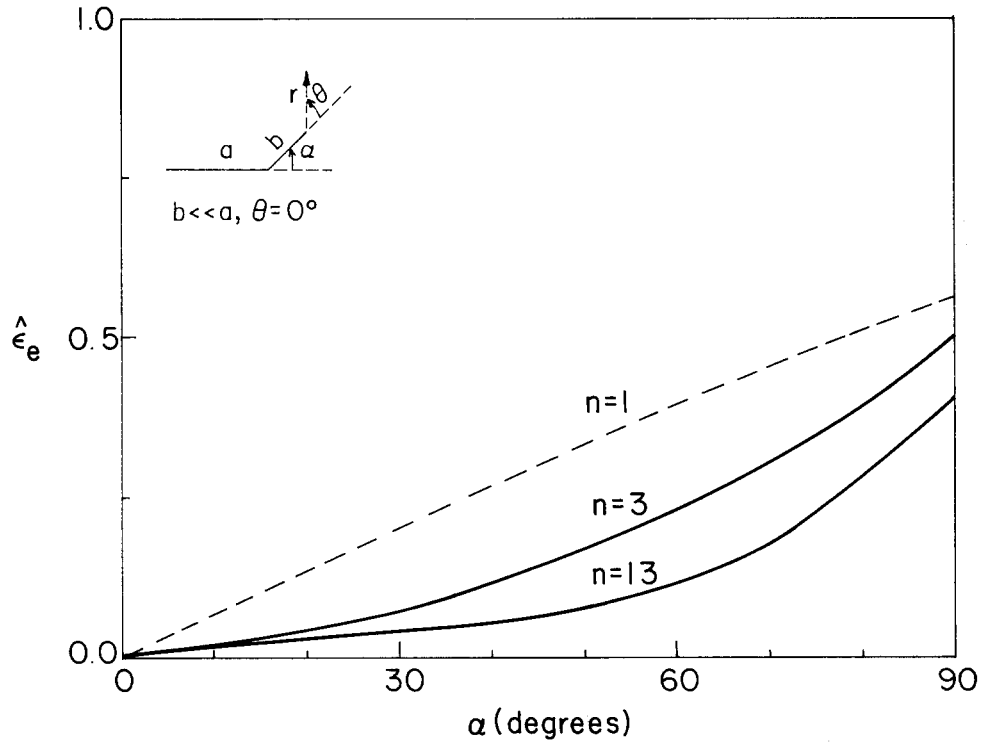

Figure 14. Variation of normalized effective strain with the branch angle α. The curve for the ideally elastic limit is indicated by the dashed line.

Thus the following provides the definition for an effective stress intensity factor

$$k_{\text{eff}} = \sqrt{k_1^2 + k_2^2}\,. \tag{5.6}$$

This is also amenable to any energy release rate interpretation under the conditions stated above. Furthermore under small scale yielding conditions J and G are equivalent. Hence

$$J = G = \left(\frac{1-\nu^2}{E}\right) k_{\text{eff}}^2. \tag{5.7}$$

The result (5.7) suggests a possible definition for the intrinsic fracture toughness k_c for a branched crack. If the criterion for crack advance is the attainment of a characteristic work of fracture (as in a Griffith-type approach), replacing k_{eff} with k_c in (5.7) defines the work of fracture. This approach does not require any information about the near-tip fields (other than the relationships between remote loading and k_1 and k_2) or the micromechanisms of fracture. In other words, the condition for fracture is determined by a critical value of k_{eff} (5.7) and does not depend on the relative mix of k_1 and k_2 as defined by M^e. On the other hand, the use of the plastic near-tip fields (as presented in Sections 3 and 4) to determine an intrinsic fracture toughness, k_c or J_c, for branched cracks would require the introduction of a specific fracture criterion e.g., the attainment of a critical stress/strain over a characteristic microstructural distance. It is not obvious that the condition for fracture can be meaningfully phrased in terms of a single (mode-invariant) value of k_c or J_c since the near-tip fields under mixed mode conditions depend additionally on the mixity parameter M^p.

The stress intensity factors k_1 and k_2 are meaningful characterization parameters when the plastic zone size, r_p, is smaller than $b/50$ where b is the length of the branch. In this

regard we emphasize that at the same value of k_{eff} (5.6), the plastic zone size under combined k_1 and k_2 fields is considerably larger than that under purely k_1 field [19,20]. Hence plasticity effects which may be insignificant for straight cracks ($\alpha = 0$) could become significant for branch cracks (or if the near-tip fields are longer mode I). We believe that the results provided in Figs. 9 through 14 could be applicable for plastic zone size, r_p, less than half the length of the branch, b. As noted previously, the quantification of the effect of near-tip plasticity on the fracture toughness requires the introduction of a fracture criterion. The specification of such a criterion for complex crack-tip geometries must be based on an understanding of the microscopic crack growth mechanisms. Therefore while the present results suggest favorable effects due to crack tip plasticity, it is presently not possible to quantify the improvement in fracture properties without a further understanding of the microstructure-dependent separation mechanisms.

Ishikawa et al. [29] and Bui [30] have proposed that the mixed mode fields be separated into mode I and mode II components. This separation can only be accomplished for linear crack problems. Their formulation does provide a direct method for the determination of k_1 and k_2. Following this line of argument, Cotterell et al. [31] introduced the notion of a failure-mode-independent fracture resistance characterization. From their work, it is not obvious as to how the separation of the work of fracture into mode I and mode II components would lead to a physical basis for such a postulate. As noted previously, the work of separation, i.e., the energy release rate, under small scale yielding conditions for coplanar crack advance is given by (5.7).

Standard procedures for the measurement of fracture initiation toughness (e.g. K_{Ic}) often involve a limited amount of crack growth, typically up to 2 percent of the uncracked ligament. Therefore, microstructurally-induced crack branching often leads to an apparently larger nominal value of the fracture initiation toughness as defined by K_{Ic} (e.g. [14]). In high toughness ductile materials, it is known that effects of microstructurally-induced branching on crack growth resistance can be even more pronounced. This has been observed in recent studies of crack growth resistance, as characterized by the tearing modulus, in lithium-containing aluminum alloys [16,32].

We emphasize that the results presented in Figs. 9 through 14 are relevant to the small scale yielding problem. The results may be expected to provide a reasonable approximation to the near-tip fields when the plastic zone size extends up to one-half the length of the kink or fork. For cases where the plastic zone engulfs the kink or the fork completely, the connection between the plastic near-tip fields as characterized by M^p and J (or K^p) and the remote boundary loads must be evaluated directly for the particular geometry and load level. In other words, the full boundary value problem must be treated. Nevertheless, the plastic crack tip fields (3.2) are universal and these fields can be embedded into a singular core element containing fields characterized by K^p and M^p. These plastic near-tip fields can be linked to the remote boundaries by conventional finite element discretization and the solution procedure can develop along the lines already discussed in [19,20] for the small scale yielding problem.

Acknowledgements

This work was supported partly by the Brown University Materials Research Laboratory under NSF Grant DMR-8316893 and partly by the NSF Grant NSF-ENG-8451092. The authors express their sincere thanks to Mrs P. Capece and Mrs L. Gray for their help in the preparation of this manuscript.

References

[1] M.A. Hussain, S.L. Pu and G. Underwood, in *Fracture Analysis* Part II, ASTM STP 560 (1974) 2–28.
[2] K. Palaniswamy and W.G. Knauss, in *Mechanics Today*, S. Nemat-Nasser, Editor, Vol. 4, Pergamon Press (1978) 87–148.

[3] B.A. Bilby and G.E. Cardew, *International Journal of Fracture* 11 (1975) 708–712.
[4] S.N. Chatterjee, *International Journal of Solids and Structures* 11 (1975) 521–538.
[5] H. Kitagawa, R. Yuuki and T. Ohira, *Engineering Fracture Mechanics* 7 (1975) 515–529.
[6] B.A. Bilby, G.E. Cardew and I.C. Howard, in *Fracture 1977*, edited by D.M.R. Taplin, Vol. 3, University of Waterloo Press (1977) 197–200.
[7] H. Kitagawa and R. Yuuki, *Ibid*, 201–211.
[8] K.K. Lo, *Journal of Applied Mechanics* 45 (1978) 797–802.
[9] B. Cotterell and J.R. Rice, *International Journal of Fracture* 16 (1980) 155–169.
[10] B. Lawn and T.R. Wilshaw, *Fracture of Brittle Solids*, Cambridge University Press (1975).
[11] F. Erdogan and G.C. Sih, *Journal of Basic Engineering* 85 (1963) 519–527.
[12] G.C. Sih, *Engineering Fracture Mechanics* 5 (1973) 365–377.
[13] K.T. Faber and A.G. Evans, *Acta Metallurgica* 31 (1983) 565.
[14] A.K. Vasudevan and S. Suresh, *Materials Science and Engineering* 72 (1985) 37–49.
[15] S. Suresh, *Metallurgical Transactions* 16A (1985) 249–260.
[16] S. Suresh, unpublished results, Brown University (1984).
[17] C.S. Carter, *Engineering Fracture Mechanics* 3 (1971) 1–13.
[18] D.R. Hayhurst, P.R. Brown and C.J. Morrison, *Philosophical Transactions Royal Society London*, A 311, (1984) 131–158.
[19] C.F. Shih, "Elastic-Plastic Analysis of Combined Mode Crack Problems", Ph.D. Thesis, Harvard University (1973).
[20] C.F. Shih, in *Fracture Analysis*, ASTM STP 560 (1974) 187–210.
[21] J.R. Rice, *Journal of Applied Mechanics* 35 (1968) 379–386.
[22] J.W. Hutchinson, *Journal of the Mechanics and Physics of Solids* 16 (1968) 13–31.
[23] J.R. Rice and G.F. Rosengren, *Journal of the Mechanics and Physics of Solids* 16 (1968) 1–12.
[24] J.K. Knowles and E. Sternberg, *Archive for Rational Mechanics and Analysis* 44 (1972) 187.
[25] B. Budiansky and J.R. Rice, *Journal of Applied Mechanics* 40 (1973) 201–203.
[26] R.M. McMeeking, *Journal of the Mechanics and Physics of Solids* 25 (1977) 357–381.
[27] J.W. Hutchinson, *Journal of Applied Mechanics* 50 (1983) 1042–1051.
[28] A.C. Mackenzie, J.W. Hancock and D.K. Brown, *Engineering Fracture Mechanics* 9 (1977) 167–188.
[29] H. Ishikawa, H. Kitagawa and H. Okamura, in *Proceedings of Third International Conference on Materials*, edited by K.J. Miller and R.F. Smith, Vol. 3, Pergamon Press, Oxford (1979).
[30] H.D. Bui, *Journal of the Mechanics and Physics of Solids* 31 (1983) 439–448.
[31] B. Cotterell, E. Lee and Y.W. Mai, *International Journal of Fracture* 20 (1982) 243–250.
[32] S. Suresh and A.K. Vasudevan, *Materials Science and Engineering* 79 (1986) 183–190.

Résumé

On met l'accent sur une procédure par laquelle on détermine les contraintes plastiques au voisinage d'extrémités de fissures en branches et les champs de déformation correspondants, sous un état plan de déformation et sous des conditions de plastification à petite échelle.

La méthode fait appel à des solutions connues pour le facteur d'intensité de contrainte, ainsi qu'aux champs plastiques de mode mixte au voisinage de l'extrémité d'une fissure pour déterminer les conditions de contrainte et de déformation à la pointe d'une fissure en fragmentation ou d'une fissure en fourche. Les champs plastiques au voisinage de l'extrémité sont caractérisés par un paramètre de mixité et par une amplitude.

On examine l'influence de la plasticité à la pointe de la fissure et les caractéristiques d'écrouissage du matériau sous les état locaux de contrainte de dilatation.

On discute de la possibilité d'effets bénéfiques d'une fissure efflorescente et de la plasticité à l'extrémité d'une fissure sur la ténacité à la rupture et sur la résistance à la croissance d'une fissure, à la lumière de ces résultats.